Multi-wall carbon nanotube coating of fluorine-doped tin oxide as an electrode surface modifier for polymer solar cells

A. Capasso[a,1], L. Salamandra[b], A. Chou[a], A. Di Carlo[b] and N. Motta[a]

[a] *School of Chemistry Physics and Mechanical Engineering, Queensland University of Technology, 2 George St, Brisbane, QLD 4000, Australia*

[b] *CHOSE (Centre for Hybrid and Organic Solar Energy), Department of Electronic Engineering, University of Rome Tor Vergata, Via del Politecnico 1, 00133 Rome, Italy*

Abstract

A controlled layer of multi-wall carbon nanotubes (MWCNT) was grown directly on top of fluorine-doped tin oxide (FTO) glass electrodes as a surface modifier for improving the performance of polymer solar cells. By using low-temperature chemical vapor deposition with short synthesis times, very short MWCNTs were grown, these uniformly decorating the FTO surface. The chemical vapor deposition parameters were carefully refined to balance the tube size and density, while minimizing the decrease in conductivity and light harvesting of the electrode. As created FTO/CNT electrodes were applied to bulk-heterojunction polymer solar cells, both in direct and inverted architecture. Thanks to the inclusion of MWCNT and the consequent nano-structuring of the electrode surface, we observe an increase in external quantum efficiency in the wavelength range 550÷650 nm. Overall, polymer solar cells realized with these FTO/CNT electrodes attain power conversion efficiency higher than 2%, outclassing reference cells based on standard FTO electrodes.

1. Introduction

Organic photovoltaics has been gaining momentum in recent years and is now one of the fastest-developing technologies in the field of green energy. Its success largely hinges upon the low manufacturing and material costs, simple fabrication via printing techniques [1],

[1] Corresponding author. Email address: a.capasso@qut.edu.au (A. Capasso).

which also opened to the creation of flexible devices by roll-to-roll processing [2, 3], providing the access of organic solar cells to market areas generally closed to silicon-based solar cells [4]. Thanks to a strong research interest, polymer solar cells have undergone a steady increase in power conversion efficiency (PCE) [5, 6], becoming a mature technology able to compete in the market [7, 8, 9].

Indium tin oxide (ITO) is a transparent conductive oxide commonly used as a standard electrode in thin film and organic photovoltaics [10]. However, its electrical/optical properties require further optimization to achieve maximum device's performance. In the past, several research groups proposed carbon nanotubes (CNT) in the cell architecture to take advantage of their superior electrical and morphological properties [11]. As for electrodes, CNT layers have been deposited on glass to replace ITO as electrode material, yet failing to attain a ratio between sheet resistance and transparency that would promote an effective replacement of ITO [12]. Hybrid configurations combining ITO and CNT proved to be a more effective strategy, albeit with a large room for improvement. Freestanding CNT sheets have been placed on top of ITO reaching 1.7% of PCE [13]. In order to exploit further such promising results, CNTs have been embedded in the cell architecture by growing them directly on the ITO surface by chemical vapor deposition (CVD), in an attempt of improving the charge collection at the electrode [14, 15]. However, the high temperature required for the CVD process (500-600°C) is extremely detrimental to the conductivity and optical transmittance of ITO [16], and thus represents a major hindrance to this approach's application. Therefore, although the direct synthesis of CNT on ITO have successfully demonstrated the possibility of using a transparent conductive oxide as CVD substrate, the overall PCE of as-built solar cells never reached values as high as the references due to the inherent incompatibility in material processing, so putting an end to this line of research.

In order to overcome such an impasse, in this article we explore for the first time the direct synthesis of CNT on fluorine-doped tin oxide (FTO). Differently from ITO, FTO can sustain a prolonged sintering at temperatures higher than 500°C without changing its properties [17]; remarkably, it has been reported even a drop in FTO's resistivity by 1Ω /sq after a thermal treatment in air at 600°C [18]. By analyzing the synthesized materials by electron microscopy and Raman spectroscopy, we investigated the impact of a wide range of CVD parameters and ultimately found the process conditions providing the best combination of conductivity and transparency for FTO/CNT electrodes. We developed polymer solar cells by using these modified FTO/CNT electrodes, finding an increased efficiency compared to the conventional architectures.

2. Experimental methods

2.1 MWCNT synthesis on FTO electrodes

MWCNT were synthesized on FTO electrodes. The glass/FTO substrates (Pilkington, 8Ω/□, 3mm/700nm thick) were cleaned by ultrasonic baths in acetone and isopropyl alcohol. A 3nm layer of Ni was deposited in high-vacuum by thermal evaporation at 10^{-6} mbar. The substrates were loaded face-down on top of a Si stage in a CVD system, where the set temperature on the stage is reached by Joule effect. The CNT synthesis was performed at 600°C for the desired time with an Ar/C_2H_2 flow (300/30 sccm). When the synthesis was complete, the samples were quickly cooled down to room temperature (fast extraction).

After CVD, the substrates were analyzed by FE-SEM (JEOL JSM-7001F) and TEM (Jeol 1011 TEM). Raman spectra were collected using an inVia Renishaw Micro-Raman system. The 632.8nm line of a He-Ne laser at room temperature were focused on an area of the samples about 1 μm wide, choosing a low laser power to prevent heat accumulation. On each sample, several areas were probed and the spectra were averaged to rule out possible discrepancies in the surface. The transmittance spectra of the electrodes were acquired with a

UV-Vis spectrophotometer (Shimadzu UV-2550). The sheet-resistance of FTO/CNT electrodes were measured with a Keithley 2410 source-meter in four-probe configuration

2.2 Solar cell assembly and testing

Bulk-heterojunction (BHJ) solar cells were built in a glove-box filled with nitrogen by using standard glass/FTO and glass/FTO/CNT electrodes. A film of *poly(3,4-ethylenedioxythiophene):poly(styrenesulfonate)* (PEDOT:PSS) was deposited by spin coating as hole transport layer between FTO and photoactive blend. This is a standard step in the polymer solar cell assembly, required to flatten the ITO surface, improve the charge collection, align the energy level and increase the V_{OC}) [11], but it is unfeasible on FTO/CNT because of the high hydrophobicity of the CNT layer. Therefore, alternate transport layers with equal performance were used to adapt the work function energy of the electrodes to the HOMO-LUMO levels of the donor/acceptor blend. Two specular configurations of polymer solar cells were implemented: inverted (electrode/Cs_2CO_3/P3HT:PCBM/MoO_3/Ag) and direct (electrode/MoO_3/P3HT:PCBM/Ca/Al). In the inverted cell, a Cs_2CO_3 electron transport layer, deposited via liquid phase processing [19,20], allows the energy level alignment between cathode and active layer; similarly, an evaporated MoO_3 [21,22] hole transport layer promotes the charge transfer between the active layer and the metal anode. In the direct cell, the MoO_3 is at the interface with transparent conductive oxide anode [23].

For the inverted cell, the 2nm layer of Cs_2CO_3 was spin-coated on glass/FTO(/CNT) cathode from a solution of 0.2 wt% in 2EE (2-ethoxyethanol) at 5000rpm for 60sec. A 2 wt% solution (1:0.7) of regio-regular P3HT (Sigma-Aldrich) and PCBM (Solenne BV) was diluted in DCB (dichlorobenzene) and spin-coated at 400 rpm for 60 sec (~100 nm), as active layer. At last, 5nm of MoO_3 and 100nm of Ag were deposited via thermal evaporation at 10^{-6} mbar, respectively as hole transport layer and top metal anode. For the direct structure, both MoO_3 and P3HT:PCBM layers were deposited as before. Finally, 20 nm of Ca and 80 nm of Al were

deposited via thermal evaporation (10^{-6} mbar) as top metal cathode. For the two architectures, 8 devices were realized. All the 16 cells have an active area of 16.6 mm^2 and were not encapsulated.

The current-voltage (J-V) characteristics of the cells were measured with a Keithley 2410 source-meter under AM1.5G (100 mW/cm^2) illumination of a Sun 2000 Class A ABET solar simulator. To measure the external quantum efficiency (EQE), the devices were illuminated by monochromatic light and the photocurrent is recorded by a Keithley 2612B source-meter. A Lot-Oriel IPCE system, comprising a Xe-arc lamp as white light source and a monochromator, was used to generate monochromatic light, whose intensity was measured using a Thorlabs UV-Enhanced FDS1010 calibrated Si photo-detector. Samples transmittance was obtained with a Shimadzu UV2020 spectrophotometer with integrated sphere.

3. Results and discussion

3.1 Electrode characterization

After the CVD synthesis, the electrode was less transparent, with a greyish layer covering the FTO area. Upon FE-SEM inspection, the FTO surface appears coated by a layer of multi-wall carbon nanotubes (MWCNTs), which are uniformly distributed all over the oxide crystals (Fig. 1a). Low CVD temperature (600°C) combined with short time (3 min) gave rise to the growth of CNT with small radius of curvature. The CNT length in this case could be controlled to a large extent, the nucleation rate on the tin oxide substrate being rather slow (as compared for instance to Si or SiO_2) [13]. As seen in the SEM micrograph, we managed to obtain short MWCNTs, which in some cases appeared to be solely nucleated. On average, the tubes had a diameter around 30 nm and are shorter than 100 nm, as confirmed by TEM analysis (Figure 1b). The low synthesis temperature led to the growth of defective MWCNTs, whose walls were in some cases partially covered by residual amorphous carbon.

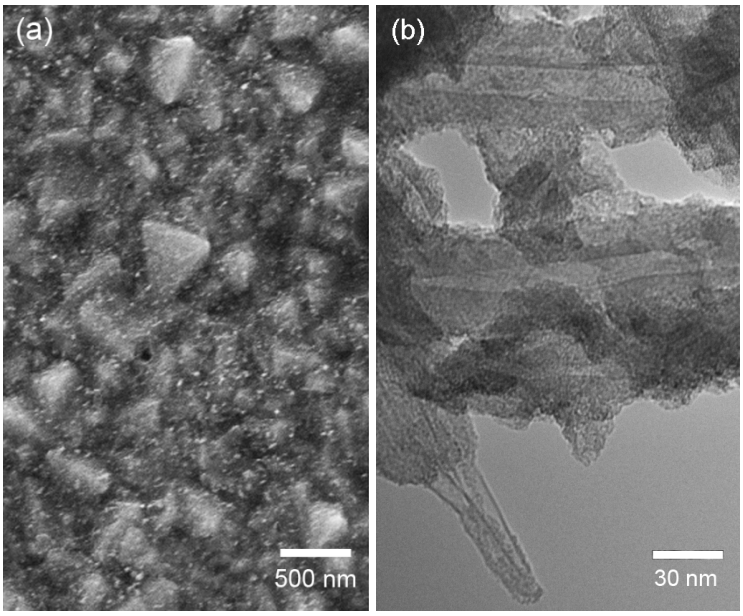

Fig. 1 – Analysis of the CNTs grown on glass FTO by CVD at 600°C in Ar/C_2H_2 (300/30 sccm). (a) SEM micrograph of the FTO/CNT electrode (3 min CVD). The surface is uniformly covered by short MWCNTs (white spots). (b) TEM micrograph of the FTO/CNT electrode (3 min CVD).

The Raman spectra taken on the FTO/CNT samples show features in the typical bands of graphitic materials as CNT (Fig. 2): D (~1350 cm^{-1}), G (~1580 cm^{-1}), and 2D (~2700 cm^{-1}). In carbon-based materials, the D band is usually attributed to defective graphitic structures (as carbonaceous impurities with sp^3 bonding, broken sp^2 bonds in the sidewalls, etc.), bending or finite-size effects [24, 25]. The G band arises from the zone center E_{2g} mode and corresponds to ordered sp^2 bonded carbon; it is enhanced in the case of carbon atoms vibrating along a nanotube axis (LO phonon mode) [26]. The 2D band is related to the iTO (in-plane transversal optical) branch in the phonon dispersion of sp^2 carbon materials [27, 28], and may represent an accurate indication of the CNT quality or purity [29].

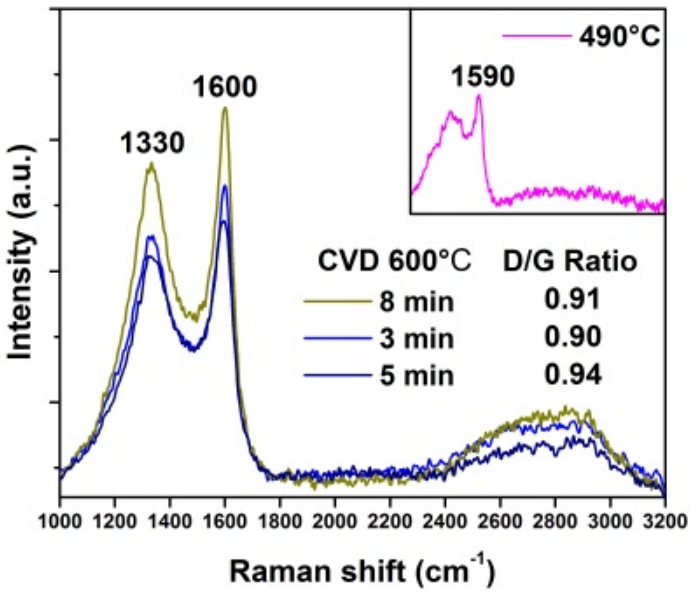

Fig. 2 – Raman spectra collected on FTO/CNT electrodes after CVD at 3, 5, 8 min, respectively (the negligible background noise in the spectra is due to the glass/FTO substrate).

For all the samples, the G peak (centered at ~1600 cm^{-1} with FWHM of 70-92 cm^{-1}) is the most intense feature but is not very sharp as in the case of single wall carbon nanotubes (SWCNT) and graphene, thus confirming the presence of MWCNTs. The peak is also shifted from 1580 to 1600 cm^{-1}, indicating the presence of graphitic layers with small crystallite sizes or abundant edges. The broad D peak (centered at ~1330 cm^{-1}) is also typical of multi-wall carbon nanotubes, which may possess defects between the various walls. The D peak shape is also coherent with the low-temperature synthesis process used (<700°C), where the available energy can usually allow only the formation of MWCNTs of large diameter (i.e. many walls), most likely with imperfect levels of graphitization and more abundant defects [30]. This inference is also supported by the presence of the (mesa-like component) weak and broad 2D mode (centered at 2780 cm^{-1}). Besides, no radial breathing modes are visible in the spectra, further proving that SWCNTs are not grown (as expected for a low-temperature CVD) and that the MWCNT diameter is quite large [31]. Overall, there seems to be a superposition between the strong MWCNT features and a background signal due to amorphous carbon

species that are likely to form as a by-product of a low temperature CVD process [32]. This is supported by the Raman spectrum of a sample processed at 490°C, shown in the inset of Fig. 2. At such a low temperature, amorphous carbon is the principal species synthesized, its spectrum being composed of a small G band peak which is smeared by a very broad D band.

The intensity ratio between D and G band peaks (I_D/I_G) can be used as an indicator of the quality on the MWNT samples, since the relative changes in the two peak intensities correlate with the amount of carbonaceous impurities in a given sample [33]. An I_D/I_G ratio of 0.9 is consistent with the low-temperature growth of CNTs and is even lower than previously reported [34], attesting the optimal choice of the CVD process conditions. The crystallite size of the grown nanographitic species, L_a (nm), can be calculated by Raman spectroscopy using the general equation $L_a = (2.4 \cdot 10^{-10})\lambda_l^4 \frac{I_G}{I_D}$, where λ_l is the laser wavelength in nm, as reported by Cancado et al. [35]. For our three samples, the equation gives graphitic domain sizes between 41-43 nm. This is consistent with the FE-SEM and TEM investigations, and also reasonable enough considering the mean Ni cluster size of a few tens of nm that is likely to coalesce at 600°C (on which the tubes nucleate).

The transmittance and measured sheet-resistance (R_S) of the different electrodes are reported in Fig. 3. The pristine glass/FTO samples show an overall transmitted power ($T_{\%}$) of 78%, in the range 300÷800 nm. After the deposition of 3nm of Ni on top of FTO, the transmittance shape changes, retaining a higher transparency at lower wavelengths, as expected for an evaporated thin metal film [36], while the overall $T_{\%}$ decreases to 65%. After the CVD, the transmittance spectrum of the new electrode (FTO/CNT) recovers the shape of pristine glass/FTO, but $T_{\%}$ is further reduced to an average value of 51% (53÷48%). As expected, the Ni's signature is no longer present in the spectrum, since the Ni layer is likely to fragment into small clusters during the CVD synthesis; these give rise to the CNT's nucleation and end up embedded in them. The transmittance spectrum of the CNT layer itself (extracted from the

spectra of glass/FTO samples with and without CNT film) is also presented for comparison. As shown in the inset in Fig. 3, the sheet-resistance of the FTO/CNT electrodes is close to that of pristine glass/FTO substrates (~8 Ω/□) and increases with the electrode opacity, which in turn reflects the CNT coverage, reaching an average value of 10.4 Ω/□ (9.7÷10.7Ω/□).

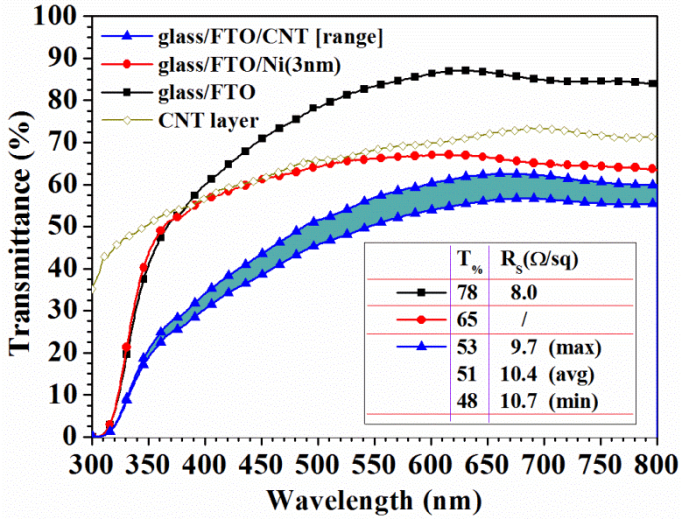

Fig. 3 - Transmittances of the different substrates: (■) bare FTO on glass; (●) FTO with 3nm layer of Ni; (▲) FTO with CNT layer (a range of possible transmittance curves are shown because the FTO/CNT electrodes slightly differs one another); (◊) transmittance of the CNT layer alone (calculated). In the inset, a table with the overall transmitted power ($T_{\%}$) and the sheet resistance of the samples are reported (see SI for details). The inverse dependence between $T_{\%}$ and R_S is apparent.

From the comprehensive characterization of our samples, some considerations can be drawn. By low temperature CVD with acetylene (at atmospheric pressure), short and sparse MWCNT can be easily grown on a transparent conductive oxide surface. The combination of surface roughness, short synthesis time and low nucleation rate hinders the formation of a dense layer of CNTs as a carpet. Moreover, in this case the van der Waals forces between such sparse nanotubes are too weak to play a role in their vertical alignment. In turn, the electrode

transmittance is retained at acceptable values. Moreover, thanks to process's short duration and the fast extraction from the heating-stage the electrodes retain a good balance between conductivity and transparency. To this extent, we have specifically avoided the use of H_2 (along with Ar) as carrier gas, because of its detrimental effect on the oxide film properties, as already reported in the case of ITO [15]. We further characterized the properties of the FTO/CNT electrodes, evaluating their work function by Kelvin Probe method. An increase of 100÷200meV (~150meV) is measured for FTO/CNT in respect to untreated FTO, similarly to the case of ITO [15]. As for the absolute values, we can refer to the work function of the tantalum probe used in the measurement (4.2 eV), indicating a value of 5.1 eV for FTO/CNT with respect to 4.9÷5.0 eV of bare FTO, in line with several reports [37, 38]. Such a modification in work function for FTO/CNT electrodes is expected to affect the performance of cells based on two different architectures.

3.2 Solar cell testing

After the substrate characterization, we selected 16 FTO/CNT electrodes with similar properties (transmittance ~51%, sheet resistance ~10.4 Ω/□) to build both inverted and direct polymer solar cells, in order to test the cell performance and investigate the CNT effect on the two cell architectures, reported in Fig. 4.

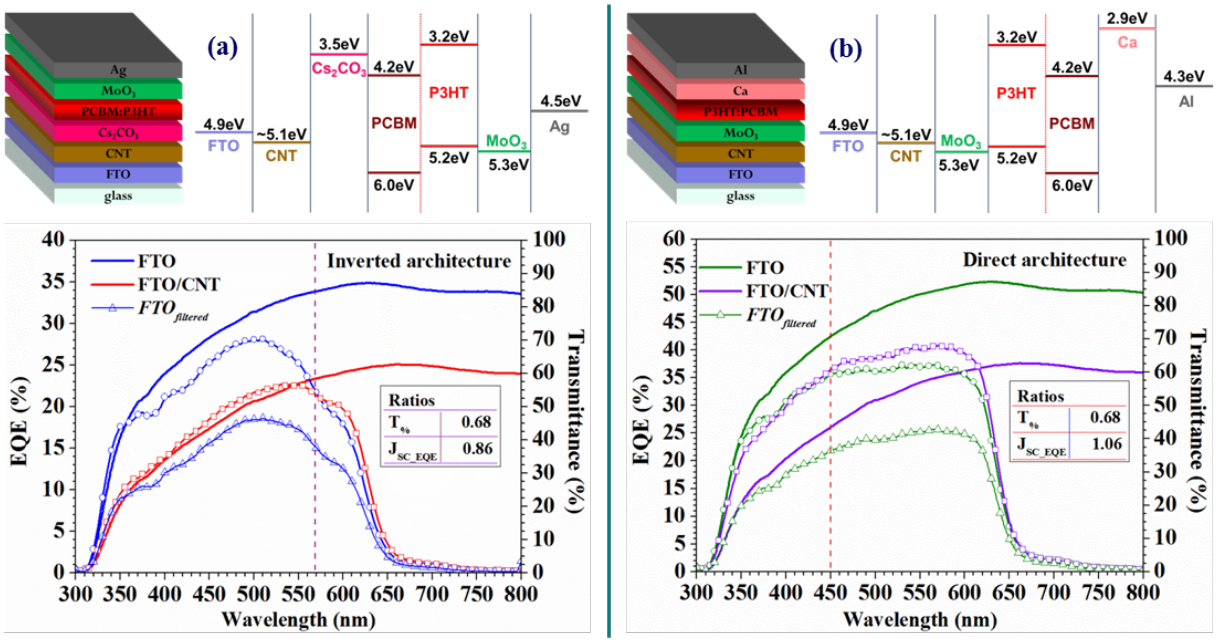

Fig. 4 - Structure scheme, energy level diagram [17,21,37,38], and EQE (symbol+line) vs Transmittance (line) comparison of the PSC architectures used in this work: (a) inverted and (b) direct. In the inset, a table with the ratio values ($T_{\%}$ and J_{SC} extracted from EQE) between FTO with and without CNT is reported.

We measured the EQE of our polymer solar cells to study the effect of the CNT layer on FTO. The graphs are shown in Fig. 4, along with the reference transmittance spectra of the electrodes (FTO and FTO/CNT). The $FTO_{filtered}$ curve in the graphs simulates the EQE of a cell made with a CNT/glass/FTO electrode, that is, a cell with an external CNT layer (an

optical filter in this case) on glass. This simulation helps in appreciating the decrease in efficiency for a cell collecting a $T_{\%}$ of only 53%, elucidating the impact of the CNT on the device properties.

It can be noted that the FTO/CNT cell with inverted architecture (Fig. 4a) presents an EQE with a different shape in respect to the reference cell, with the maximum downshifted at 550 nm. The EQE has lower values in the wavelength range $300<\lambda<570$ nm, but outperforms the reference cell at $\lambda>570$ nm. Overall, the average decrease in EQE is not as severe as it should be for a cell electrode with a $T_{\%}$ of 53%, as remarked by the $FTO_{filtered}$ curve, which is much lower the FTO/CNT itself (max of 18% vs 24%, respectively).

Interestingly, the FTO/CNT cell with direct architecture shows an EQE higher than the reference almost throughout the whole range 300-800 nm (Fig. 4b). The two spectra have a similar shape, but the EQE of FTO/CNT cell rises markedly over the reference in the range $\lambda>450$ nm.

In order to understand the possible contribution of CNT to the cell performance, it is useful to remind that the EQE derives from the product of the light transmitted to the cell and four efficiencies corresponding to each step in the charge generation process: photon absorption, exciton diffusion, exciton dissociation and charge collection [39]. The absorption efficiency, related to the composition and processing of the photoactive material, should stay the same in all our experiments, while the exciton dissociation efficiency can be in general treated as unity. Consequently, the EQE improvement for the FTO/CNT cells, considering also their lower transmittance, can be in principle related to higher efficiency in exciton diffusion or charge collection, or to a combination of both. However, the exciton diffusion is mostly related to the segregation of donor and acceptor domains, and a thin and sparse layer of CNT can hardly affect the blend formation process (besides, the active layer is deposited on top of the buffer layers and not directly on the CNT surface). Therefore, in our understanding, the

inclusion of CNT in the cell architecture aids in particular the charge collection process, which is also the charge generation step depending the most on the interfaces formed between photoactive layer and electrodes. The charge extraction might also be facilitated by the additional electric field created by the MWCNTs [40]. The contribution of the MWCNTs to such an electrical optimization is particularly intense at lower photon energies (i.e. λ>450 nm). In order to quantify this effect, we extracted the J_{SC} from the EQE curves (J_{SC_EQE}) and calculated the J_{SC} ratio between the FTO/CNT and the FTO cell. These values (shown in the table in Fig 4, for both architectures) are compared to the $T_{\%}$ ratio of the two cells (0.68). For the inverted structure, the J_{SC_EQE} ratio is 0.86, confirming that the CNT are able to offset the decrease in transmittance by improving the charge collection. For the direct structure, the J_{SC_EQE} ratio is much higher and more than 1 (~1.06).

In particular, the remarkable increase in EQE provided by the FTO/CNT electrode to the direct cell could be explained by an additional effect of the CNT layer, not related to its favored morphology: The FTO/CNT electrode is expected to have an increased work function, and this would ease the hole collection by providing an improved energy level alignment with the hole transport layer (MoO_3).

In this framework, it seems likely that the CNT coating on FTO, although partially decreasing the transmitted power to the active layer, may have a twofold, positive effect on the cell's electrical properties: i) creating nanostructured paths on the electrode able to collect charge carriers closer the point of generation/separation in the photoactive layer; ii) favoring the band energy alignment in the direct cell. Overall, the inclusion of CNT has a beneficial effect on the EQE, especially in the direct architecture, by improving the charge carrier collection at the electrode and possibly, to a lesser extent, the exciton diffusion efficiency.

Fig. 5 shows the J-V curves of the realized devices measured under an illumination of 1 sun (AM1.5G); the electrical parameters are reported in Table 1.

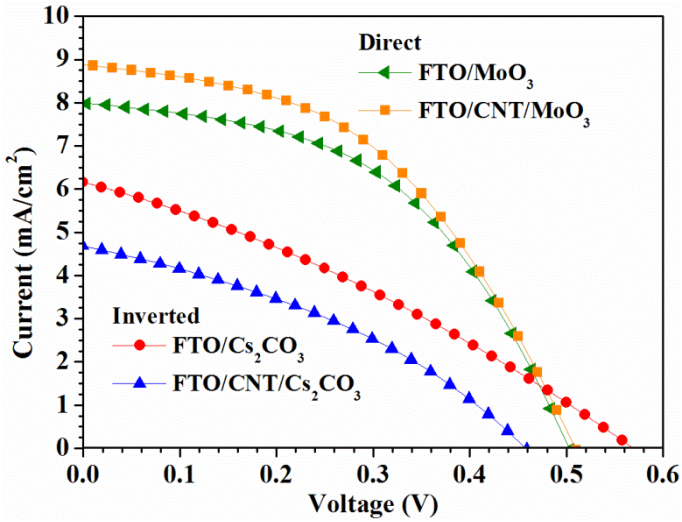

Fig. 5 - J-V curves of the solar cells realized with different architectures: (●) FTO/Cs_2CO_3, (▲) $FTO/CNT/Cs_2CO_3$, (◀) $FTO/CNT/MoO_3$, (■) $FTO/CNT/MoO_3$.

As can be noted, the inverted cell made with FTO/CNT shows a decrease of both V_{OC} (106 mV less) and J_{SC} (1.4 mA/cm^2 less), which leads to a PCE of 0.8%, as opposed to 1.1% of the reference. However, the decrease in PCE is not large, considering the low $T_{\%}$ of the FTO/CNT electrode (32% less than the FTO cell). The current density remains relatively high thanks to the improved charge carrier collection at the FTO/CNT surface.

The situation drastically changes for the solar cell made with direct architecture. In this case the J_{SC} increases by more than 10% while the V_{OC} and FF remain constant; therefore, the FTO/CNT cell outperforms the FTO one, so attesting a PCE of 2.1% (vs 2.0%). Such a result is highly significant for cells made with electrodes with a $T_{\%}$ of around 50%.

Solar Cell Architecture	V_{OC} (mV)	J_{SC} (mA/cm^2)	FF (%)	PCE (%)	J_{SC_EQE} (mA/cm^2)
FTO/Cs_2CO_3	566	6.09	32	1.1	5.01
$FTO/CNT/Cs_2CO_3$	460	4.69	36	0.8	4.32
FTO/MoO_3	504	7.99	49	2.0	8.05
$FTO/CNT/MoO_3$	510	8.88	46	2.1	8.56

Table 1 - Electrical parameters of both inverted and direct architectures of organic solar cells made with or without CNTs on top of FTO.

These results confirm our speculation about the energy band level of the FTO/CNT electrodes. Indeed, a work function increased to 5 eV has an opposite effect on energy band alignment of the two different cell architectures: in an inverted cell, the inclusion of the CNT layer between FTO and Cs_2CO_3 is likely to add a higher energy barrier for electrons, thus lowering the device's electrical performance (essentially V_{OC}, see figure 4a); conversely, a direct cell with FTO/CNT should benefit from an anode work function closer to the energy level of the hole transport layer (5.3 eV for MoO_3), thus reducing the hole collection losses (figure 4b).

4. Conclusion

We successfully modified the surface of FTO by directly growing CNTs at low temperature on top of it. Optimal CVD parameters were selected, making it possible to obtain a uniform yet transparent MWCNT coating while preserving the FTO conductivity. We built and tested direct and inverted solar cells with FTO/CNT electrodes to elucidate the effect of CNT on two cell architectures with opposite band energy alignment. The CNT coating on the FTO increased the EQE of the cells, mainly on the account of an improved charge carrier collection to the electrode. In the direct architecture, the beneficial impact of the CNTs can be not only related to the nano-structuring of the electrode, but also connected to a more favorable energy-band alignment between FTO/CNT and photoactive blend.

ACKNOWLEDGEMENTS

The authors acknowledge the financial support of the ARC through the Discovery project DP130102120, the Marie Curie International Research Staff Exchange Scheme Fellowship

within the 7th European Community Framework Programme, and the Project "Polo Solare Organico – Regione Lazio". A warm thanks goes to Regis Anghilante for his help in the electrode preparation.

References

1. Moulé, A.J., *Power from plastic.* Current Opinion in Solid State and Materials Science, 2010. **14**(6): p. 123-130.
2. Krebs, F.C., *Polymer solar cell modules prepared using roll-to-roll methods: Knife-over-edge coating, slot-die coating and screen printing.* Solar Energy Materials and Solar Cells, 2009. **93**(4): p. 465-475.
3. Krebs, F.C., M. Jørgensen, K. Norrman, O. Hagemann, J. Alstrup, T.D. Nielsen, et al., *A complete process for production of flexible large area polymer solar cells entirely using screen printing—First public demonstration.* Solar Energy Materials and Solar Cells, 2009. **93**(4): p. 422-441.
4. Krebs, F.C., S.a. Gevorgyan, B. Gholamkhass, S. Holdcroft, C. Schlenker, M.E. Thompson, et al., *A round robin study of flexible large-area roll-to-roll processed polymer solar cell modules.* Solar Energy Materials and Solar Cells, 2009. **93**(11): p. 1968-1977.
5. He, Z., C. Zhong, S. Su, M. Xu, H. Wu and Y. Cao, *Enhanced power-conversion efficiency in polymer solar cells using an inverted device structure.* Nature Photonics, 2012. **6**(September): p. 591-595.
6. You, J., L. Dou, K. Yoshimura, T. Kato, K. Ohya, T. Moriarty, et al., *A polymer tandem solar cell with 10.6% power conversion efficiency.* Nature communications, 2013. **4**: p. 1446-1446.

7. Sommer-Larsen, P., M. Jørgensen, R.R. Søndergaard, M. Hösel and F.C. Krebs, *It is all in the Pattern-High-Efficiency Power Extraction from Polymer Solar Cells through High-Voltage Serial Connection.* Energy Technology, 2013. **1**(1): p. 15-19.
8. Shrotriya, V., *Organic photovoltaics: Polymer power.* Nature Photonics, 2009. **3**(8): p. 447-449.
9. Chen, C.-c., L. Dou, R. Zhu, C.-h. Chung, T.-b. Song, Y.B. Zheng, et al., *Visibly transparent polymer solar cells produced by solution processing.* ACS nano, 2012. **6**(8): p. 7185-90.
10. Nelson, J., *Polymer:fullerene bulk heterojunction solar cells.* Materials Today, 2011. **14**(10): p. 462-470.
11. Hoppe, H. and N.S. Sariciftci, *Organic solar cells: An overview.* Journal of Materials Research, 2004. **19**(7): p. 1924-1945.
12. Pasquier, A.D., H.E. Unalan, A. Kanwal, S. Miller and M. Chhowalla, *Conducting and transparent single-wall carbon nanotube electrodes for polymer-fullerene solar cells.* Applied Physics Letters, 2005. **87**(20).
13. Ulbricht, R., S.B. Lee, X. Jiang, K. Inoue, M. Zhang, S. Fang, et al., *Transparent carbon nanotube sheets as 3-D charge collectors in organic solar cells.* Solar Energy Materials and Solar Cells, 2007. **91**(5): p. 416-419.
14. Miller, A.J., R.A. Hatton, G.Y. Chen and S.R.P. Silva, *Carbon nanotubes grown on In[sub 2]O[sub 3]:Sn glass as large area electrodes for organic photovoltaics.* Applied Physics Letters, 2007. **90**(2): p. 023105-3.
15. Capasso, A., L. Salamandra, A.D. Carlo, J.M. Bell and N. Motta, *Low-temperature synthesis of carbon nanotubes on indium tin oxide electrodes for organic solar cells.* Beilstein Journal of Nanotechnology, 2012. **3**: p. 524-532.
16. Ginley, D.S., *Handbook of Transparent Conductors.* 2011, Boston, MA: Springer US.

17. Beshkov, G.D., K.M. Kolentsov, D.B. Dimitrov, L.S. Yourukova, A.S. Rachkova and M.T. Kamenova. *Effect of high-temperature treatment in different ambient on the properties of SnO2:F*.

18. Zardetto, V., T.M. Brown, A. Reale and A. Di Carlo, *Substrates for flexible electronics: A practical investigation on the electrical, film flexibility, optical, temperature, and solvent resistance properties.* Journal of Polymer Science Part B: Polymer Physics, 2011. **49**(9): p. 638-648.

19. Park, Y., S. Noh, D. Lee, J. Kim and C. Lee, *Study of the Cesium Carbonate (Cs2CO3) Inter Layer Fabricated by Solution Process on P3HT:PCBM Solar Cells.* Molecular Crystals and Liquid Crystals, 2011. **538**(1): p. 20-27.

20. Liao, H.H., L.M. Chen, Z. Xu, G. Li, and Y. Yang, *Highly efficient inverted polymer solar cell by low temperature annealing of Cs_2CO_3 interlayer*. Applied Physics Letters, 2008. **92**(17): p. 173303.

21. Liu, F., S. Shao, X. Guo, Y. Zhao and Z. Xie, *Efficient polymer photovoltaic cells using solution-processed MoO3 as anode buffer layer.* Solar Energy Materials and Solar Cells, 2010. **94**(5): p. 842-845.

22. Zhao, D.W., S.T. Tan, L. Ke, P. Liu, A.K.K. Kyaw, X.W. Sun, et al., *Optimization of an inverted organic solar cell.* Solar Energy Materials and Solar Cells, 2010. **94**(6): p. 985-991.

23. Shrotriya, V., G. Li, Y. Yao, C.-W. Chu and Y. Yang, *Transition metal oxides as the buffer layer for polymer photovoltaic cells.* Applied Physics Letters, 2006. **88**(7): p. 073508-3.

24. Duesberg, G.S., I. Loa, M. Burghard, K. Syassen and S. Roth, *Polarized Raman Spectroscopy on Isolated Single-Wall Carbon Nanotubes.* Physical Review Letters, 2000. **85**(25): p. 5436-5439.

25. Stankovich, S., D.A. Dikin, R.D. Piner, K.A. Kohlhaas, A. Kleinhammes, Y. Jia, et al., *Synthesis of graphene-based nanosheets via chemical reduction of exfoliated graphite oxide.* Carbon, 2007. **45**(7): p. 1558-1565.

26. Dresselhaus, M.S. and G. Dresselhaus, *Intercalation compounds of graphite.* Advances in Physics, 1981. **30**(2): p. 139-326.

27. Maultzsch, J., S. Reich and C. Thomsen, *Double-resonant Raman scattering in graphite: Interference effects, selection rules, and phonon dispersion.* Physical Review B, 2004. **70**(15).

28. Pimenta, M.A., G. Dresselhaus, M.S. Dresselhaus, L.G. Cancado, A. Jorio and R. Saito, *Studying disorder in graphite-based systems by Raman spectroscopy.* Physical Chemistry Chemical Physics, 2007. **9**(11): p. 1276-1290.

29. Saito, R., A. Gruneis, G.G. Samsonidze, V.W. Brar, G. Dresselhaus, M.S. Dresselhaus, et al., *Double resonance Raman spectroscopy of single-wall carbon nanotubes.* New Journal of Physics, 2003. **5**.

30. Kim, C.D., H.S. Jang, H.R. Lee and D.H. Kim, *Low temperature growth of carbon nanotubes in a magnetic field.* Materials Letters, 2007. **61**(10): p. 2075-2078.

31. Datsyuk, V., M. Kalyva, K. Papagelis, J. Parthenios, D. Tasis, A. Siokou, et al., *Chemical oxidation of multiwalled carbon nanotubes.* Carbon, 2008. **46**(6): p. 833-840.

32. Chu, P.K. and L.H. Li, *Characterization of amorphous and nanocrystalline carbon films.* Materials Chemistry and Physics, 2006. **96**(2-3): p. 253-277.

33. DiLeo, R.A., B.J. Landi and R.P. Raffaelle, *Purity assessment of multiwalled carbon nanotubes by Raman spectroscopy.* Journal of Applied Physics, 2007. **101**(6).

34. Ziebro, J., I. Lukasiewicz, E. Borowiak-Palen and B. Michalkiewicz, *Low temperature growth of carbon nanotubes from methane catalytic decomposition over nickel supported on a zeolite.* Nanotechnology, 2010. **21**(14).

35. Cancado, L.G., K. Takai, T. Enoki, M. Endo, Y.A. Kim, H. Mizusaki, et al., *General equation for the determination of the crystallite size L-a of nanographite by Raman spectroscopy.* Applied Physics Letters, 2006. **88**(16).

36. Sennett, R.S. and G.D. Scott, *The Structure of Evaporated Metal Films and Their Optical Properties.* J. Opt. Soc. Am., 1950. **40**(4): p. 203-210.

37. Helander, M.G., M.T. Greiner, Z.B. Wang, W.M. Tang and Z.H. Lu, *Work function of fluorine doped tin oxide.* Journal of Vacuum Science & Technology A, 2011. **29**(1).

38. Wei, X., T. Xie, D. Xu, Q. Zhao, S. Pang and D. Wang, *A study of the dynamic properties of photo-induced charge carriers at nanoporous TiO(2)/conductive substrate interfaces by the transient photovoltage technique.* Nanotechnology, 2008. **19**(27): p. 275707.

[39] Forrest, S.R., *The limits to organic photovoltaic cell efficiency*. MRS Bulletin, 2005. **30**(1): p. 28–32.

[40]. El Khakani, M.A., V. Le Borgne, B. Aissa, F. Rosei, C. Scilletta, E. Speiser, et al., *Photocurrent generation in random networks of multiwall-carbon-nanotubes grown by an "all-laser" process.* Applied Physics Letters, 2009. **95**(8): p. 083114-3.